J. Phys. D: Appl. Phys. 55 (2022) 265002 (6pp)

https://doi.org/10.1088/1361-6463/ac62a1

Magnetostatic coupling effects on reversal dynamics

Hao Chen¹, So Young Jeon^{1,2} and Sara A Majetich^{1,*}

E-mail: sara@cmu.edu

Received 17 February 2022, revised 23 March 2022 Accepted for publication 30 March 2022 Published 8 April 2022



Abstract

The effects of magnetostatic coupling on switching dynamics are investigated for assemblies of patterned disc-shaped magnetic elements using mumax³ micromagnetic simulations. The arrangements of coupled dots were designed using information about the switching fields and reversal dynamics of isolated dots, as well as the magnitude of the magnetic stray fields they generate. The magnetization dynamics for individual dots was examined during a reversal cascade down a linear chain of dots. The magnetization angle fluctuated much more when neighboring dots have opposite magnetization directions, consistent with a lower energy barrier for reversal. The data were analyzed to differentiate thermal and interaction field effects. While many systems of interacting nanomagnets have been analyzed in terms of empirical models, the dynamical energy barrier approach offers a methodology with a more detailed and physically intuitive way to study both simple systems like the chain and more complex assemblies such as artificial spin ice.

Supplementary material for this article is available online

Keywords: micromagnetism, magnetization dynamics, magnetization switching, superparamagnetism

(Some figures may appear in colour only in the online journal)

1. Introduction

Interacting nanomagnets are known to have more complex dynamics than isolated monodomain nanoparticles. An *isolated* particle may be magnetically stable and switched deterministically, as described by the Stoner–Wohlfarth model [1]. Alternatively it could be superparamagnetic if thermal fluctuations are sufficient to reorient the magnetic moment direction within the measurement time. In this case Néel–Brown theory applies to the net magnetization of an ensemble of non-interacting particles as a function of temperature and magnetic field, and the magnetization relaxes exponentially in time

[2–4]. With interactions, the anisotropic and long-range nature of the magnetostatic field generated by a nanomagnet leads to a broad range of relaxation times for nearby nanomagnets. In strongly interacting systems the magnetic relaxation can even be logarithmic in time [5]. Time and frequency-dependent measurements are the most sensitive way to probe the interactions [6]. The AC susceptibility shows Vogel–Fulcher (VF)-like behavior in the χ " loss peak temperature, which has been associated with a spin freezing temperature analogous to the Blocking temperature for superparamagnets [7–10]. The term superferromagnet is sometimes used to refer to thermally fluctuating clusters of particles above the spin freezing temperature [11]. These systems are also referred to as super-spin glasses because of the distribution in relaxation times, though the sharp cusp in the magnetization versus temperature has

¹ Physics Department, Carnegie Mellon University, Pittsburgh, PA 15213, United States of America

² Department of Physics, Boston University, Boston, MA 02215, United States of America

^{*} Author to whom any correspondence should be addressed.

not been reported. While most assemblies of monodomain nanoparticles have some magnetic frustration due to the spatial anisotropy of the dipolar field, in artificial spin ice (ASI), magnetic frustration is engineered through the geometry of the periodic nanopatterns [12–16]. ASI has a blocking transition between a frozen and liquid-like fluctuating state that has been modeled by a VF relation [17] or stretched exponential [18] distribution of relaxation times [19].

For both nanoparticle assemblies and nanopatterns of ASI, magnetostatic interactions lead to changes in the magnetization dynamics. While there are models that can fit the experimental data, they also reduce very complex behavior to a small number of empirical parameters, and have underlying assumptions that are not always valid. For non-interacting particles, the Néel-Brown-Arrhenius law gives a characteristic relaxation time $\tau = \tau_0 \exp{[E_0/k_BT]}$, where the inverse attempt rate τ_0^{-1} is known to within an order of magnitude, and corresponds physically to the Larmor precession time, and the energy barrier E_0 depends on the anisotropy and particle volume. The magnetization M then relaxes at a rate \sim exp $[-t/\tau]$. The VF law has similar exponential relaxation, except that $\tau = \tau_{\rm VF} = \tau_0 \exp{[E/k_{\rm B} (T-T_0)]}$. Here the energy barrier E includes the average interaction energy E_{int} as well as E_0 , and T_0 is the spin freezing temperature τ_0 , E_{int} , and T_0 are fitting parameters. The argument of the exponential in the VF formula arises from assuming a statistical distribution of interaction fields that contribute to a Langevin function, and taking the first order in the series expansion [17]. In the stretched exponential approach, and the related Cole-Davidson model [20], $M \sim \exp\left[-(t/\tau_{\rm SE})^{\beta}\right]$, and the exponential factor is the integral of $\exp[-t/\tau]$ weighted by a distribution of relaxation times. This distribution rises sharply near the endpoints of the shortest ($\tau = 0$) and longest (τ_{max}) relaxation times in the ensemble, and a relatively flat distribution in between [21]. In the Street and Woolley model of magnetic viscosity [5], which has been used to explain the slow relaxation dynamics in magnetic recording media [22], the distribution of energy barriers is assumed to be flat between maximum and minimum values.

Improved computational and experimental methods [23] enable detailed monitoring of fast dynamics within individual particles of an assembly. A more detailed quantitative understanding of the dynamics will be useful in designing interacting nanomagnets for applications such as short-term memory for magnetic logic [24–30], reservoir computing [31–34] and fast magnonic devices [35]. As interest increases in more complex systems, there is a need for improved methodology. In particular, the energy barrier distribution and its relative population over time will impact the relaxation dynamics. In this paper we describe an approach using simple arrangements of nanoparticles and their distribution of switching times. The data are analyzed to quantitatively differentiate effects from thermal and magnetostatic energies. We show for a single temperature how interactions change the energy barrier distribution and relaxation dynamics, for a nanomagnet within a chain, and for an example with magnetic frustration.

2. Simulations of non-interacting magnetic nanodots

The first issues addressed were the effects of size and ellipticity of the dots, which determines their coercivity H_c and the role of thermal fluctuations at 300 K. We began with mumax³ [36–38] simulations for isolated nanodots, where the length and width of the dots were varied and the thickness was kept constant at 3 nm. The material parameters were typical of cobalt iron boron (saturation magnetization of $8.0 \times 10^5 \mathrm{A \, m^{-1}}$, exchange stiffness of $2.2 \times 10^{-11} \text{J m}^{-1}$, and a Gilbert damping constant α of 0.03). Mesh sizes were calculated in each simulation such that the cell size was between 2 to 3 nm. The steepest conjugate gradient method was used to minimize the energy of the system. The maximum change in magnetization required to stop the iterations was set to a fractional difference of 1×10^{-11} between each step. The simulations were run for 150 ns with a 10 ps time step. Simulations were repeated using 20 different thermal seeds. The coercivity of individual noninteracting dots was determined by simulating the influence of an external applied field. The magnitude of this field was varied and the system was allowed to equilibrate. The process was repeated to scan a range of fields, once while stepwise increasing and once while decreasing the field magnitude. The step size was decreased from 50 to 10 Oe near the anticipated coercivity, and five trials were averaged for increased precision. We wanted the dots to have a monodomain ground state, but not to be superparamagnetic, on the time scale of the simulations. Coercivity increases as the measurement time is reduced, and here the effective measurement time is ~ 100 ns. Magnetometry typically involves measurement times ~ 100 s, where the nanomagnets studied here would be deemed superparamagnetic. However, for interest in future studies of fast dynamics, such as applications in magnonics, smaller patterns are desirable. The ellipticity of the dots introduces shape anisotropy, producing a non-zero coercivity. Figure 1 shows the average magnetization of the dot along the external field for a representative 70×65 nm elliptical dot, which had a coercivity of approximately 34 Oe. The results of multiple dimensions of dots showed that the coercivity of dots increased with ellipticity as expected. The coercivity also decreased with the overall size of the dot, as the device is leaving the coherent rotation-like regime, and reversal proceeds by nucleation and domain wall motion [23]. The results are summarized in table S1 (available online at stacks.iop.org/JPhysD/55/265002/mmedia).

3. Simulations of a chain of interacting nanodots

We selected the 70×65 nm size to study the effect of magnetostatic interactions based on the requirement of moderate thermal stability, at least on short time scales, and the need to generate a net field comparable to H_c in neighboring dots. Future experimental work will use spin orbit torque to initiate the magnetization dynamics of the interacting dots (IDs) by switching a larger control dot nearby. A simpler approach was used for the simulations, but also involved a control dot. The

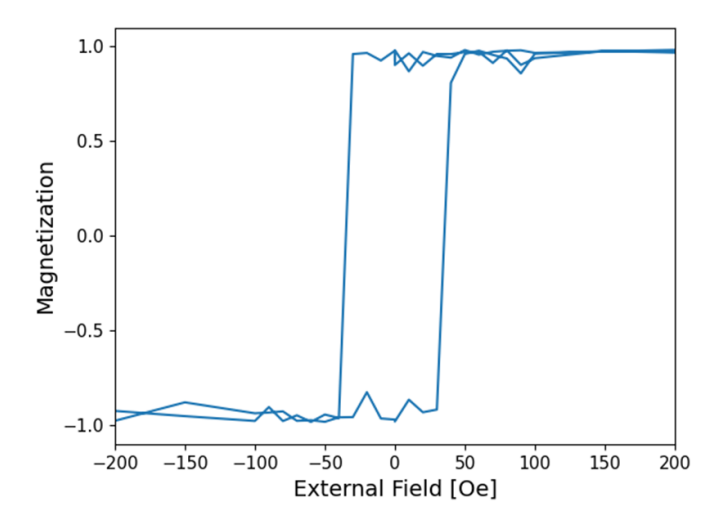


Figure 1. Hysteresis loop simulation of a 70×65 nm elliptical dot. The coercivity of this dot is approximately 34 Oe. The simulation was equilibrated for 1 ns for each step.

Figure 2. A 160×80 nm control dot is used to switch a series of thirty 70×65 nm secondary dots, all with an edge-to-edge spacing of 20 nm. In order to prevent thermally induced reversal on the right end of the chain, there is a separate 100×65 nm blocking dot set off by a 40 nm spacing. An external field of 15 Oe was applied in the +x direction in order to grow the reversed domain in the control dot. This image shows a snapshot in time of the chain of dots. See video S1 in supplemental material for a video of the dots as they fluctuate and switch over time in the reversal cascade.

elongated control dot was a rectangle merged with circles on each end. The inter-dot spacing is constrained by lithography to be ≥ 20 nm and impacts the strength of the magnetostatic coupling and the speed of reversal along the chain. Figure 2 shows a schematic of the control dot and chain of 30 secondary dots. The large number of dots was used to obtain improved statistics on switching, and to determine the conditions for a cascade of reversal in the secondary dots, which would be relevant for magnetostatic fringe field $H_{\rm fringe}$ due to a uniformly magnetized dot was calculated as a function of distance in the x-direction, which is along the chain of particles in the final simulations. The system was relaxed at 300 K before recording the magnetostatic field, and the results are analyzed based on 20 trials using different thermal seeds.

Figure 3 shows the magnetostatic fringe field of a control dot along the direction of the chain of secondary dots. For a fixed aspect ratio, the magnitude of the fringe field increases with the dot size, but the effect is small, as shown in figure S1.

The coercivity of the control dot exceeds that of the secondary dots, which makes it harder to distinguish the effect of magnetostatic coupling from that of an external field. We were able to reduce the magnitude of the external field by artificially nucleating a circular reversed region at one end of the control dot. The simulation was run at different values of the

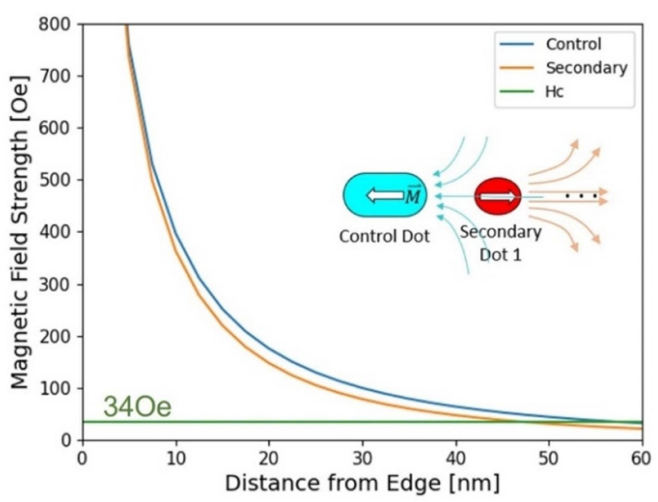


Figure 3. Fringe field of a 160×80 nm elliptical control dot, increasing distance from the edge of the dot in the *x*-direction. The fringe field was measured on a line parallel to the *x*-axis and centered with the dot in the *y* and *z* directions. The coercivity of a 70×65 nm secondary dot is shown as a comparison. The fringe field of the control dot will be strong enough to flip the secondary dot up to ~ 50 nm away.

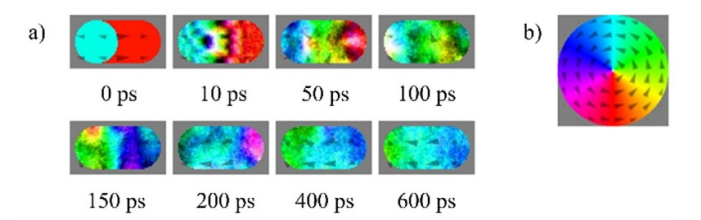


Figure 4. (a) Snapshots of simulation of a 160×80 nm dot with a reversed domain nucleation region, switching entirely under a 15 Oe external field in the x direction. The total time shown is 600 ps. (b) Color code for the magnetization direction of the images of part (a), as well as for other simulation results.

external magnetic field to determine the lowest external magnetic field needed to switch the dot. Figure 4 shows images of the magnetization pattern as a function of time.

The lowest external magnetic field required to switch the dot increased with the x length of the elongated dot. The results of the 160×80 nm dot suggest that the results are proportional to the ratio of x and y lengths rather than the size of the dot. The results are summarized in table S2.

Next we optimized the conditions such that the reversal of the control dot creates a fringe field that initiates a cascade of switching in the chain of secondary dots. There needs to be a large difference in the fringe field of the control dot and the secondary dot, which can be achieved by increasing the size of the control dot and/or by decreasing the size of the secondary dots. $|H_{\rm ext}|$ must be less than the coercivity of secondary dot 1 and greater than the minimum field needed to grow the reverse domain nucleation region in the control dot. Another observation was that thermal fluctuations were occasionally sufficient to initiate reversal from the right-hand end of the chain. This problem was solved through the addition of a 100×65 nm

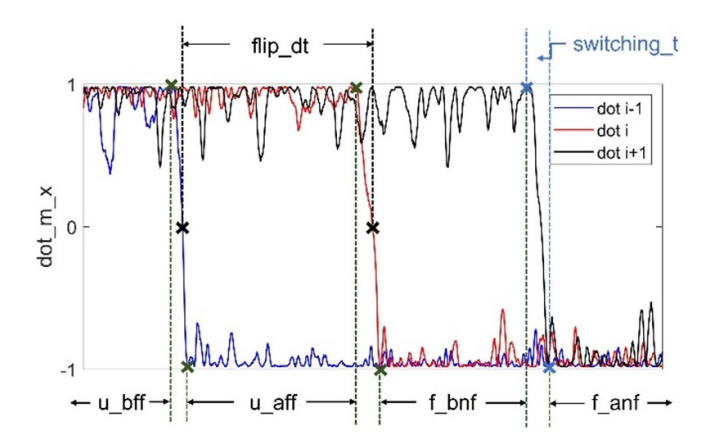


Figure 5. Normalized m_x (dot_m_x) as a function of time for one of the secondary dots, showing a typical switching event. There are four distinct time regions when the dot magnetization is fluctuating but not switching: (a) when neither dot i nor dot (i-1) has switched (u_bff), (b) after dot (i-1) has switched but not dot i (u_aff), (c) after dot i has switched but before the dot (i+1) (f_bff), and (d) after dot (i+1) has switched and dot i is part of the flipped chain (f_aff). The time of a switching even is shown as switching_t, and the time between switches in adjacent dots is flip_dt.

unreversed blocking dot with a 40 nm gap relative to the rightmost secondary dot.

4. Analysis of reversal dynamics of interacting nanodots

In order to analyze the results more quantitatively, we considered the magnetization of each secondary dot of figure 2 as a function of time t. With the chain oriented along the x-axis, we define the average magnetization m_x and m_y for each dot i, and an angle $\theta = \arctan(m_y/m_x)$ The time of a switching event is determined from the plots of $m_x(t)$, as shown in figure 5. The normalized m_x fluctuates about +1 when the dot is magnetized in the +x direction before a switch, and then about -1 afterward. The time of a switching event is defined as when m_x crosses through zero. Omitting the duration of the switching event, the time trace for dot i can be divided into four regions.

These time regions were determined for each of the 30 secondary dots, and then used to plot histograms showing the distribution of θ before and after reversal, as shown in figure 6. To obtain good statistics and minimize artifacts, the simulations were repeated with 20 different thermal seed values. The distributions are Gaussian, and centered around $\theta=0$ before switching and around $\theta=\pi$ afterward. The distribution is narrower when the neighbors on either side of the dot are both unswitched (u_bff), or after both are switched (f_anf). When the neighbors are in different states (u_aff or f_bnf), there is an additional field-induced destabilization on top of the thermal fluctuations.

We also examined the variation in the duration of switching events for dots along the chain, as shown in figure S2. While there is some arbitrariness in establishing the precise boundaries, there was no obvious pattern to the duration of a switching

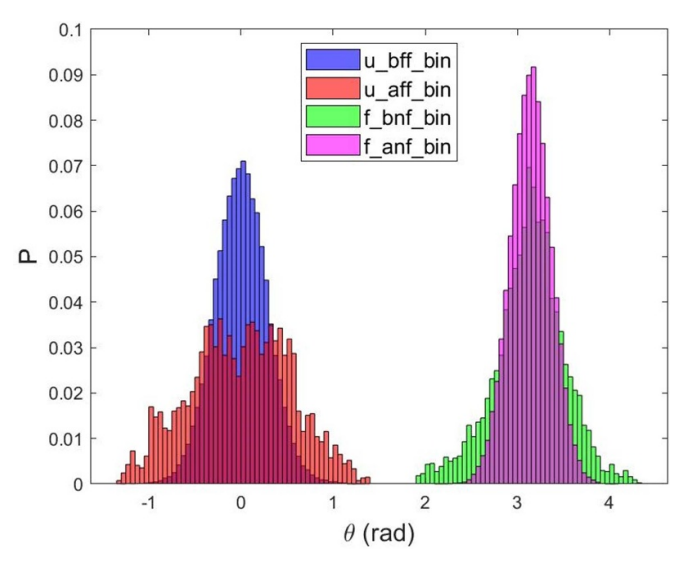


Figure 6. Probability P as a function of average magnetization angle θ for the 30 dots, averaged over the four different time regions specified above, for the conditions shown in figure 2.

event. It takes an average of \sim 400 ps to switch the magnetization from the +x to the -x direction.

5. Model of interactions

The Boltzmann method is then applied to further understand the distribution of the magnetization within each time region, where different full width half maxima (FWHM) are observed. For simplicity we used a coherent rotation model where the energy of an elliptical dot could be written as the sum of the Zeeman energy and the shape anisotropy energy, where $E = E_z + E_A$. The Zeeman energy is defined as $E_z =$ $-\mu_0 HMV \cos \theta$, where μ_0 is the vacuum permeability, H is the total external field, M is the saturation magnetization, V is the volume of the elliptical dot device and θ is the angle between the device magnetization and the external field H. In the dot chain case of figure 2, we can approximate the fringe field generated by the two closest neighbors, and the add the applied 15 Oe field to estimate the total field H. The effective field generated by one closest neighbor is estimated as the average field over the device area, where $H_{\text{eff}} = \frac{\int H_x dS}{\int dS} = 37$ Oe, and the H values or the four different time regions are shown schematically in figure 7. The shape anisotropy energy is defined as $E_A = -\frac{\mu_0}{2} M^2 (N_b - N_a) V \cos^2 \theta + C$, where N_b and N_a are demagnetizing factors for an elliptical thin film dot along the minor axis and major axis, and C is a constant only related to the shape of the device [39]. The distribution of magnetization directions, characterized by angle θ , should then follow a Boltzmann distribution $\sim \exp{-\frac{E(\theta)}{k_{\rm B}T}}$, where $k_{\rm B}$ is the Boltzmann constant and the temperature $T=300{\rm K}$. The distribution peaks at $\theta = 0$, where the energy of the system is minimized. The boundary of the FWHM (θ_b) could be found by solving $\frac{1}{2} = \frac{\exp(-E(\theta)/k_BT)}{\exp(-E(0)/k_BT)}$, and FWHM = $2|\theta_b|$. The theoretical prediction of the FHWMs for time region 1-4 are: 0.562, 2.01, 0.816, and 0.483 radians, respectively. The corresponding simulation results were: 0.65, 1.5, 0.75, and 0.55.

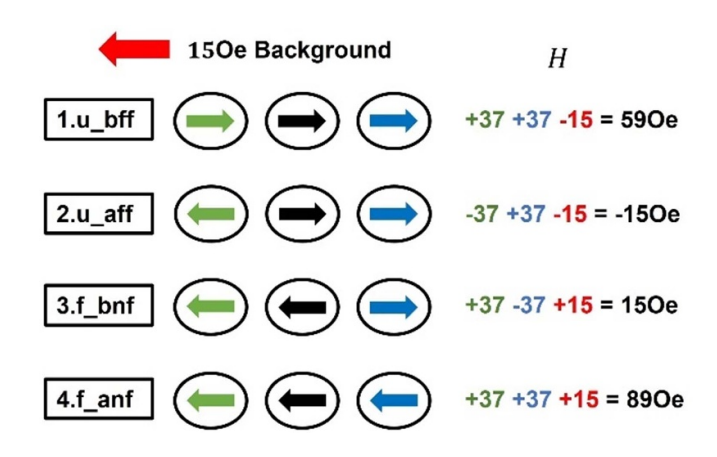


Figure 7. Total effective field for the four different time regions of figure 5. The signs are determined by whether the field is parallel or antiparallel to the magnetization of the investigated dot.

The Boltzmann law dictates the distribution when the system is at a relatively stable state, driven by thermal fluctuations.

Mumax³ simulations are based on the Landau-Lifschitz-Gilbert equation rather than an energy barrier model. To translate the simulation results into energy barrier models with and without interactions, we first considered an isolated nanopattern with a coherent rotation energy barrier dominated by shape anisotropy, in a 15 Oe external field like that shown in figure 7. Using 20 simulations with different thermal seeds, we calculated probability that the magnetization of the dot is not switched at time t, and fit to an exponential function, $P(t) = \exp(-t/\tau)$ [40], to determine $\tau = \tau_{\text{isolated}} =$ 5.63 ns. Using this value, we estimated the appropriate value for the attempt frequency, τ_0^{-1} . Here anisotropy was assumed to be dominated by shape anisotropy, and the resulting energy barrier contribution was $E_K = \mu_0 KMV = 5.56k_BT$. The magnetostatic field due to the 15 Oe external field decreased the total energy barrier energy barrier E_{Tot} by $E_{\text{ms}} = \mu_0 HMV =$ $3.1k_{\rm B}T$. The inverse attempt frequency is then estimated to be $\tau_0 = \exp(E_{\text{Tot}}/k_{\text{B}}T)/\tau_{\text{isolated}} = 0.482 \text{ ns}, \text{ consistent with res-}$ ults from previous work [40-43]. We assume that the attempt frequency did not change when the nanomagnets interact. Using this τ_0 and the P(t) fit for the interacting chain of dots, the characteristic ID relaxation time $\tau_{\text{ID}} = 3.97 \text{ ns}$ (figure 8), corresponding to a total energy barrier of $E_{\text{Tot,ID}} = 2.11k_{\text{B}}T$. The interaction energy contribution to the barrier was therefore $E_{\text{ID}} = E_{\text{Tot,ID}} - E_{\text{Tot}} = -0.35k_{\text{B}}T$.

Simulations showed that the smaller dots of figure 2 were stable for at least 3 μ s unless the control dot switched. Only with the control dot reversal, and corresponding change in the magnetostatic fringe fields to reduce the energy barrier, do the smaller dots switch within this time. Obviously, deviations from the coherent rotation model and long-range interactions also modify the energy barrier, but the results suggest that the interacting moments of the nanomagnets are effectively frozen at 300 K over this time period unless the neighboring moments point in opposite directions. In contrast, in the VF model, $E_{\rm ID} = E_{\rm int} < E_0$, so we are in the weak interaction regime of Shtrikman and Wohlfarth [17],

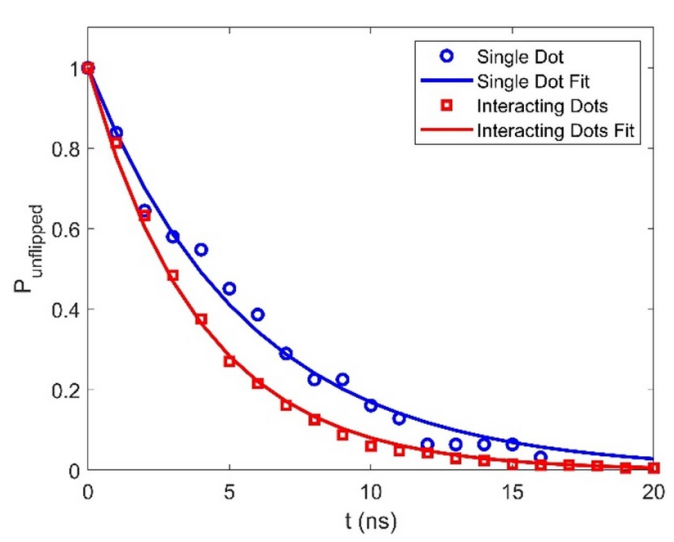


Figure 8. Comparison of simulation and exponential fits for the probability that a nanodot has not reversed, as a function of time.

where the spin freezing temperature $T_0 = E_{\rm int}^2/k_{\rm B}E_{\rm K} = 6.6$ K. The large discrepancy arises because the VF model considers an average interaction field, while in the cascading chain of dots, the energy barrier is reduced for one dot at a time.

This approach could be extended to ASI systems, with geometries such as that shown in figure S3, leading to numerous possible interaction fields that evolve over time as the system relaxes. There would be a larger number of distinct energy barriers, compared with two for the chain of dots. There could be multiple relaxation pathways, but by adding their rates, the overall relaxation could be modeled. For the short-term memory and magnonic applications proposed for ASI, the key feature is not overall relaxation to a ground state but propagation of excitations, and to realize these possibilities it will be important to understand how the spatial distribution of energy barriers varies over time.

6. Conclusions

Micromagnetic simulations were used to investigate magnetostatic effects on the reversal of a magnetostatically coupled chain of dots. These elliptical nanopatterns were designed to be stable on a microsecond time scale, but to switch in a cascade when triggered by reversal of a larger control dot. The average magnetization angle for a given dot fluctuated in time, with a Gaussian distribution about the most stable state. The FWHM of the distribution was much larger during the time period when the two adjacent dots had moments in opposite directions, temporarily reducing the energy barrier. A small external field was used to break symmetry and favor the sequential cascade of reversal. While the time of the actual switching events was short (\sim 0.4 ns), the characteristic relaxation time τ was much longer, and reflected the local energy barrier to reversal. The results can be interpreted in terms of an Arrhenius law model, where the energy barrier varies spatially and dynamically. We demonstrate for the simple case of a chain of dots that the effects of magnetostatic interactions can be accounted for without requiring changes in the attempt frequency or an unphysical spin freezing temperature. This same approach has potential application to more complex systems such as ASI.

Data availability statement

The data that support the findings of this study are available upon reasonable request from the authors.

Acknowledgments

S A M acknowledges support from NSF Grant ECCS-2004559.

ORCID iDs

Hao Chen https://orcid.org/0000-0001-7693-0245 So Young Jeon https://orcid.org/0000-0003-1266-5029

References

- [1] Stoner E C and Wohlfarth E P 1948 *Phil. Trans. R. Soc.* A 240 599
- [2] Neel L 1959 J. Phys. Radium 20 215
- [3] Brown W F Jr 1963 Phys. Rev. 130 1677
- [4] Coffey W T and Kalmykov Y P 2012 J. Appl. Phys. 112 121301
- [5] Street R and Woolley J C 1949 Proc. Phys. Soc. A 62 562
- [6] Majetich S A and Sachan M 2006 J. Phys. D: Appl. Phys. 39 R407
- [7] Zhang J, Boyd C and Luo W 1996 *Phys. Rev. Lett.* 77 390
- [8] Mørup S 1994 Hyperfine Interact. 90 171
- [9] Petracic O, Chen X, Bedanta S, Kleemann W, Sahoo S, Cardoso S and Freitas P P 2006 J. Magn. Magn. Mater. 300 192
- [10] Peddis D et al 2021 Sci. Rep. 11 7743
- [11] Yamamoto K, Majetich S A, McCartney M R, Sachan M, Yamamuro S and Hirayama T 2008 Appl. Phys. Lett. 93 082502
- [12] Wang R F et al 2006 Nature 439 303
- [13] Farhan A, Derlet P M, Kleibert A, Balan A, Chopdekar R V, Wyss M, Perron J, Scholl A, Nolting F and Heyderman L J 2013 Phys. Rev. Lett. 111 057204
- [14] Farhan A et al 2019 Sci. Adv. 5 eaav6380
- [15] Macauley G M, Paterson G W, Li Y, Macêdo R, McVitie S and Stamps R L 2020 Phys. Rev. B 101 144403

- [16] Östman E, Stopfel H, Chioar I, Arnalds U B, Stein A, Kapaklis V and Hjörvarsson B 2018 Nat. Phys. 14 375
- [17] Shtrikman S and Wohlfarth E P 1981 Phys. Lett. 85 467
- [18] Williams G and Watts D C 1970 Trans. Faraday Soc. 66 80
- [19] Morley S A, Alba Venero D, Porro J M, Riley S T, Stein A, Steadman P, Stamps R L, Langridge S and Marrows C H 2017 Phys. Rev. B 95 104422
- [20] Havriliak S and Negami S 1967 Polymer 8 161
- [21] Chowdary K M and Majetich S A 2014 J. Phys. D: Appl. Phys. 47 175001
- [22] Lu P L and Charap S H 1994 J. Appl. Phys. 75 5768
- [23] Parks B, Abdelgawad A, Wong T, Evans R F L and Majetich S A 2020 *Phys. Rev. Appl.* **13** 014063
- [24] Cowburn R P and Welland M E 2000 Science 287 1466
- [25] Imre A, Csaba G, Ji L, Orlov A, Bernstein G H and Porod W 2006 Science 311 205
- [26] Li Z and Krishnan K M 2017 J. Appl. Phys. 121 023908
- [27] Nakatani R, Nomura H and Endo Y 2009 J. Phys.: Conf. Ser. 165 012030
- [28] Bhowmik D, You L and Salahuddin S 2013 *Nat. Nanotechnol.*
- [29] D'Souza N, Fashami M S, Bandyopadhyay S and Atulasimha J 2016 Nano Lett. 16 1069
- [30] Arava H, Derlet P M, Vijayakumar J, Cui J, Bingham N S, Kleibert A and Heyderman L J 2018 Nanotechnology 29 265205
- [31] Skjaervø S H, Marrows C H, Stamps R L and Heyderman L J 2020 *Nat. Rev. Phys.* 2 13
- [32] Nomura H, Furuta T, Tsujimoto K, Kuwabiraki Y, Peper F, Tamura E, Miwa S, Goto M, Nakatani R and Suzuki Y 2019 Jpn. J. Appl. Phys. 58 070901
- [33] Nomura H, Tsujimoto K, Goto M, Samura N, Nakatani R and Suzuki Y 2020 Jpn. J. Appl. Phys. 59 SEEG02
- [34] Zhou P, McDonald N R, Edwards A J, Loomis L, Thiem C D and Friedman J S 2020 arXiv:2003.10948
- [35] Krawczyk M and Grundler D 2014 J. Phys.: Condens. Matter 26 123202
- [36] Vansteenkist A, Leliaert J, Dvornik M, Helsen M, Garcia-Sanchez F and van Waeyenberge B 2014 AIP Adv. 4 107133
- [37] Leliaert J, Mulbers J, de Clercq J, Coene A, Dvornik M and van Waeyenberge B 2017 AIP Adv. 7 125010
- [38] Exl L, Bance S, Reichl F, Schrefl T, Stimming H P and Mauser N J 2014 J. Appl. Phys. 115 17D118
- [39] Chang H and Burns J 2004 J. Appl. Phys. 37 3240
- [40] Wernsdorfer W, Orozco E B, Hasselbach K, Benoit A, Barbara B, Demoncy N, Loiseau A, Pascard H and Mailly D 1997 Phys. Rev. Lett. 78 1791
- [41] Kaplakis V, Arnalds U B, Farhan A, Chopdekar R V, Balan A, Scholl A, Heyderman L J and Hjörvarsson B 2014 Nat. Nanotechnol. 9 914
- [42] Farhan A, Derlet P, Kleibert A, Balan A, Chopdekar R V, Wyss M, Anghinolfi L, Nolting F and Heyderman L J 2013 Nat. Phys. 9 375
- [43] Bedanta S and Kleemann W 2008 J. Phys. D: Appl. Phys. 42 013001